Spatiotemporal organization of sleep spindles and their cross-frequency coupling in the primate cerebral cortex

Saori Takeuchi

Doctor of Philosophy

January 2015

Department of Physiological Sciences

School of Life Science

The Graduate University for Advanced Studies

Contents

Abstract

The neural mechanism of information processing during sleep is a current topic of investigation. Recent studies have suggested that cross-frequency coupling (CFC) between the neural oscillations may serve as a mechanism to transfer information in large-scale brain networks. In human studies, it is reported that sleep spindles are correlated with slow-wave phase, and that sleep spindle density is increased after learning. These findings may lead to the idea that sleep spindles and their CFC are related to memory processing. However, our present knowledge is insufficient and further evidence about sleep spindles is needed.

In this study, I have focused on the following questions: 1) How is the cortical distribution of spindles? 2) Are there multiple rhythm generators for spindles? 3) How are multi-regional spindles temporally organized? 4) How is the coupling of spindles and slow oscillations? 5) Are there triggers for generating spindles?

Electrodes were implanted into the cerebral cortex (areas 9, 46, 8, 6, 4, 1, 5, 7, 32, and 24) of three macaque monkeys (*Macaca fuscata*). They were arranged in pairs, with one of each pair at the surface and the other at a depth of the cortex. Cortical field potentials were recorded from freely behaving monkeys via telemetry, and their oscillatory properties during sleep were analyzed using Fourier analysis and Hilbert-Huang transform.

Electrical current sources of spindles were identified on widespread regions of the frontoparietal cortex. The frequencies of spindles were topographically distributed on the cortex. The fastest spindles (>15 Hz) were found in the dorsolateral prefrontal cortex (areas 46 and 8a), while the slowest ones (<14 Hz) appeared in the mesial frontal cortex (areas 32 and 24). Spindles of intermediate frequency (14-15 Hz) were

distributed in the centroparietal and medial prefrontal cortices. There was a significant tendency that spindles in different regions occurred concordantly, although the majority of spindles occurred independently. The concordance rate was relatively high between bilaterally symmetrical regions and between nearby regions. The spindles in the dorsolateral cortex tended to occur approximately at the same time and preceded the spindles in the mesial regions with a time lag of about 0.5 s. The frequencies of concurrent and non-concurrent spindles were compared across various pairs of recording sites. In the majority of the recording sites, the frequency was not affected by concurrent spindles in other regions, and spindles of different frequencies were simultaneously generated. However, in some of the pairs between bilaterally symmetrical regions and between nearby regions, the frequency of concurrent spindles was shifted as compared to that of non-concurrent spindles and/or showed a significant positive linear correlation with each other. Spindles in the lateral anterior tended to start on the positive phase of slow waves (0.1-1 Hz), while spindles in the centroparietal and the mesial frontal areas occurred around the negative phase. The phase angle of slow waves was reversed between the central region and the prefrontal region. By analyzing the time-frequency distribution calculated by Hilbert-Huang transform, an increase of gamma band activity before the spindle onset was found. The onset time of gamma activity was −0.29±0.14 s (mean±SD) as measured from the spindle onset in each area, and lasted about 0.5 s.

The present study showed that spindles in widespread cortical regions are driven by their own rhythm sources, nevertheless they are temporally and spatially related with spindles in other areas, and that they are correlated with slow waves and gamma oscillations. Because the prominent inter-spindle correlations were found

between the bilaterally symmetrical regions and between the nearby regions, corticocortical connections and crossed projections between the thalamus and the cortex or thalamic reticular nucleus may play a significant role in the spatiotemporal correlations of spindles. The cross-frequency couplings suggest that the triggering system for spindles is linked with slow waves and gamma oscillations. Because the gamma increase is limited within a short time region around the spindle onset, they may serve as a direct trigger of spindles. The interactions shown in the present study may serve as a functional basis to transfer information in large-scale brain network during sleep.

Introduction

The brain processes information not only during wakefulness but also during sleep. For example, sleep consolidates memory and enhances motor skill learning (Rasch and Born 2013). Although the detailed neural mechanism of such information processing is still unclear, the process may be partly reflected on electroencephalographic patterns during sleep, such as sleep spindles, k-complexes, and slow waves.

Sleep spindles

Sleep spindles are short bursts of waxing and waning rhythmic waves (11-16 Hz) in human electroencephalogram (EEG), named by Loomis et al. in 1935 (Loomis et al. 1935). They often occur with k-complexes during non-rapid eye movement (NREM) sleep stage 2 (N2) and with slow oscillations during slow wave sleep (SWS) (Rechtschaffen and Kales 1968).

All sleep spindles may not be of the same nature. Topographical difference in the frequency is reported in human studies (Jankel and Niedermeyer 1985; Jobert et al. 1992; Werth et al. 1997; Zeitlhofer et al. 1997). These studies suggested the existence of two types of spindles, namely, the faster spindles on the centroparietal cortex, and the slower ones on the frontal cortex. Intracranial EEG recordings in epileptic patients showed that the faster centroparietal spindles (13-15 Hz) often preceded the slower ones (9-12 Hz) in the frontal region with a time lag of about 0.2-0.5 s (Andrillon et al. 2011, Mölle et al. 2011).

Sleep spindles and slow or gamma oscillations

Spindles and slow oscillations below 1 Hz are organized in space and time (Mölle et al. 2002). In human subjects, fast spindles in the centroparietal region ride on the positive phase of slow waves, while slow spindles in the anterior middle region ride on the negative phase of slow waves (Mölle et al. 2011). It is reported that slow waves themselves are traveling waves that occur more frequently on the frontal cortex and propagate from the medial anterior to posterior (Massimini et al. 2004), and that they occur locally (Nir et al. 2011).

Gamma oscillations (30-120 Hz) are found on the neocortex and in the hippocampus of humans and animals during both sleep and wakefulness (Buzsáki and Wang 2012; Takeuchi et al. 2015; Wang 2010). In human, cortical gamma oscillations are reported during SWS, although the power is higher in rapid eye movement (REM) sleep than in SWS (Gross and Gotman 1999; Valderrama et al. 2012). Phase-amplitude coupling of gamma activity with the spindle rhythm is reported in the human (Ayoub et al. 2012).

Recent studies have suggested that cross-frequency coupling (CFC) between the neural oscillations may serve as a mechanism to transfer information in large-scale brain networks (Canolty and Knight 2010). However, the coupling of spindles with slow and gamma oscillations has rarely been studied.

Sleep spindles and memory

Several lines of evidence have indicated that spindles may be related to the consolidation of declarative and procedural memory. In human studies, the increase of spindle density after learning (Fogel and Smith 2011; Gais et al. 2002; Schabus et al. 2006), especially during SWS (Cox et al. 2012) is reported. Essentially the same

phenomenon has been reported also in rodents (Eschenko et al. 2006). Furthermore, it is reported that auditory closed-loop in-phase stimulation of slow waves during SWS enhances slow oscillation rhythms, phase-coupled spindles, and the consolidation of declarative memory (Ngo et al. 2013).

In the two-stage model of memory consolidation, two separate memory stores are assumed, namely, temporal and long-term stores (Squire 1992). Although the detailed mechanism for memory transfer between two stores is still unclear, the different functions for REM sleep and NREM sleep have been proposed (Diekelmann and Born 2010; Peigneux et al. 2001; Rasch and Born 2013). According to the sequential hypothesis of memory consolidation, recently encoded memory representations are reactivated and stored in both the temporary and long-term storages on the cortex during SWS for integration into long-term memory, while REM sleep stabilizes transformed memories. In agreement with the hypothesis, correlation between the cortical activities (spindles and slow waves) and the hippocampal high gamma oscillations (ripples) are reported in SWS of the rodent (Sirota et al. 2003). In SWS of the monkey, activation of wide cortical regions in relation to hippocampal ripples is reported using functional magnetic resonance imaging (Logothetis et al. 2012).

Problems and what to do

These findings may lead to the idea that sleep spindle is a part of larger phenomena that involve both slow (<1 Hz) and gamma oscillations and is related to memory processing. However, our present knowledge is still insufficient and further evidence is necessary to clarify the whole situation about sleep spindles. In this study, I will investigate the following five questions by recording field potentials directly from

the monkey cortex using implanted electrodes during natural sleep via telemetry system: 1) How is the cortical distribution of spindles? 2) Are there multiple rhythm generators for spindles? Two models are possible to explain the faster and slower spindles. One model is that a single rhythm generator drives multiple cortical current sources with changing the frequency. The other is that multiple rhythm generators drive multiple cortical current sources separately. 3) How are multi-regional spindles temporally organized? 4) How is the coupling of spindles and slow oscillations? 5) Are there triggers for generating spindles?

Materials and Methods

Subjects

The experiment was conducted on three adult Japanese monkeys (*Macaca fuscata*, one male (MA) and two females (MB and MC), 6-8 kg) in accordance with the National Research Council/Institute for Laboratory Animal Resources Guide for the Care and Use of Laboratory Animals, as approved by the institutional ethics committee of National Institute of Natural Sciences. The present data were recorded as a part of a larger study protocol for other purposes.

Surgical operation

Electrodes were implanted into the cerebral cortex (areas 9, 46, 8, 6, 4, 1, 5, 7, 32, and 24) (Fig. 1) under ketamine (5 mg/kg administered intramuscularly) and pentobarbital sodium anesthesia (the initial dose 25 mg/kg, administered intravenously, followed by additional injections as needed). They were made of silver wire (diameter 0.2 mm) coated with Tefron. They were cut obliquely (45 degrees) at the tip and the cross-section surfaces were served as contacts. They were arranged in pairs, with one of each pairs at the surface (S) and the other at a depth (D) of 2.5-3.5 mm in the recording sites (Fig. 1B), and were fixed to the skull by acrylic resin and screws. Electrooculogram (EOG) electrodes were buried in the superolateral part of the orbital bone and control electrodes were set in the marrow of the parietal bones behind both ears. Electromyogram (EMG) electrodes were made of two Teflon-insulated 7-strand stainless steel wires (each wire rod diameter 0.05 mm, external diameter including the coating 0.23 mm), whose coating was peeled off 5 mm from the tip, and were subcutaneously placed on the posterior nuchal muscles (the distance between electrodes

was 20 mm).

Recording

Monkeys could move freely in their cages and slept during approximately 10:00 p.m.-6:00 a.m. Light in the room was turned off during 9:00 p.m.-8:00 a.m. From two weeks after the surgery, cortical field potentials, EOG, and EMG were recorded using a telemetry system (time constant, 1 s; high-cut filter, 200 Hz; sampling rate, 500 Hz; 16 channels). The control electrodes were connected together and were used as a reference. The behavioral condition of monkeys during nights was monitored by infrared video cameras. Each video frame held time stamp to synchronize with telemetric data for offline analysis.

Sleep stage classification

Data were segmented into 20 s epochs, and were visually classified into stage of REM sleep, NREM sleep stages 1-4 (N1, N2, N3, and N4), and wakefullness in a standard manner used for human sleep classification (Rechtschaffen and Kales 1968).

Automatic detection of sleep spindles

By preliminary visual inspection of data, waxing and waning sinusoidal 12-20 Hz oscillations of about 1 s duration were often appeared in NREM sleep stages, and were often preceded by k-complexes (Fig. 2A).

Candidate sleep spindles were detected using the following procedures according to the previous human study (Andrillon et al. 2011): 1) S−D field potentials were band-pass (12-20 Hz) filtered; 2) the envelope was calculated using Hilbert

transform; 3) spindles were detected when the envelope exceeded the threshold level of the mean+3SD of the envelope; 4) START and END of spindles were defined to be the time points where the envelope crossed the mean+SD level.

To confirm that the electric currents of the spindles were generated at the recording site and were not a result of current spreading from distant cortical regions, the relative phase of S signal as referenced by D signal was calculated for the band-pass filtered signals at the every peak of D signal. Spindles were accepted when the mean phase angle during the interval from START to END was in antiphase (180±90 degrees), and otherwise rejected.

To avoid false detection caused by wide frequency band events, frequency of candidate spindles was examined on a time-frequency distribution. The time-frequency distribution was calculated by Hilbert-Huang transform (Huang 2005; Huang et al. 1998), and the resulted time-dependent Hilbert amplitude spectra were mapped on the plane whose frequency axis was divided into 200 logarithmic bins from 0.1 to 125 Hz. Then, a Gaussian filter with a full width at half maximum of 10 bins × 20 ms was applied to the map. Based on the time frequency distribution, marginal spectra were calculated for every fourth segment of the time region between START and END. Spindles were accepted when all the four spectra reached local maxima within the range of 12-20 Hz, and otherwise rejected. Spindles that passed all the aforementioned criteria were regarded as significant spindles and were provided for further analysis in the present study.

Frequency of sleep spindles

In order to determine frequency of individual spindles, marginal spectra from

START to END were calculated using the time-frequency distribution, and the frequency at which the spectrum reached the maximum was measured within the range of 12-20 Hz.

Temporal order of multiple sleep spindles

In order to examine temporal relationship of spindles between different cortical regions, cross-correlogram of START pulses was calculated for all available combination of recording sites. To estimate the probability density function of occurrence of spindle, the cross-correlogram was smoothed using a Gaussian kernel with a full width at half maximum of 0.5 s. Significance of correlation was statistically evaluated using the mean and SD of randomly shuffled same data.

The time lag of peaks in the cross-correlogram gives information about how spindles in one recording site tend to precede or follow those in the other site. In order to estimate the timing sequence of spindles in the whole recording sites using the telemetric data which covered only subset of the recording sites simultaneously, I assumed that the time lags are constant. By repeatedly measuring the time lags for all available combination of recording sites across days, simultaneous linear equations are constructed. I collected sufficient number of data, so that the equations became an overdetermined system. The best estimate of relative time lags between whole recording sites are determined by a least-squares method.

Ratio of concordant spindles between separate regions

The statistical significance in the above cross-correlogram is not a quantitative measure for the rate of concordant spindles. For quantitative evaluation about how

many spindles were appeared in a correlated manner between different recording sites, concordance index Q was defined as $Q = \frac{N_{AB} \times 2}{N_A + N_B}$, where N_A and N_B are the total number of spindles in two recording sites A and B, and N_{AB} is the number of spindles in A that occurred in a correlated manner with spindles in B. N_{AB} is calculated as the area exceeding the mean line under the peak in the cross-correlogram within the time interval in which the cross-correlogram exceeds the mean+2SD line. The value of Q ranges between 0 and 1, and $Q=1$ indicates a complete correlation where all the spindles in A and B take place in a correlated manner, while $Q=0$ indicates that none of spindles are correlated.

Frequency of concurrent spindles

In order to examine whether spindle frequency is affected by other spindles that are generated in different regions, the frequency of concurrent spindles was compared to that of non-concurrent spindles, and the null hypothesis of no effect was tested by two-way analysis of variance (ANOVA) using recording site and concurrency as main factors. In addition, linear correlation of frequency between concurrent spindles was assessed using Pearson product-moment correlation coefficient, and the null hypothesis of no linear correlation was tested. In either case, the statistical results were assessed at significance level of 5%. Two spindles were regarded as concurrent when their START-END intervals were overlapped.

Cross-frequency coupling between spindles and slow waves

To figure out slow potential shifts around sleep spindles, S−D potentials aligned at each START of spindle were averaged. In addition, in order to analyze

phase-amplitude coupling between spindles and slow waves, I measured the phase of slow waves (0.1-1 Hz) at each START of spindles. The analysis was carried out using exclusively the time regions in which the phase of slow waves was reversed between S and D. The instantaneous phase of slow waves was calculated using Hilbert transform.

Phase relationship between slow waves

The phase relationship of slow waves (0.1-1 Hz) was examined between various recording sites. S−D, S, and D potentials were separately band-pass (0.1-1 Hz) filtered using Fourier transform, and their instantaneous phases were calculated using Hilbert transform. To minimize the effects of current spreading, the phase difference between two S−D potentials was calculated, exclusively for the data segments in which slow wave phases are reversed (180±90 degrees) between S and D.

Statistical analysis of phase angle

For statistical analysis of phase locking, the null hypothesis of uniformity for the phase angle was tested using the Rayleigh statistic (Lord Rayleigh 1880), $R=\frac{|\sum \boldsymbol{r}|}{\sum|\boldsymbol{r}|}$, where $\boldsymbol{r}$ is a unit vector of phase angle. The value of R ranges from 0 to 1, and $R=1$ indicates complete phase locking.

Cross-frequency coupling between spindles and gamma oscillations

In order to examine amplitude-amplitude coupling between gamma oscillations and spindles, the time-frequency distribution was averaged separately at the time point of START of spindle and at the timing of the peak amplitude of the envelope (PEAK). The result is normalized to the z-score using surrogate time-frequency distribution

calculated from randomly sampled non-spindle regions of the same data. To determine the timing of gamma increase, time dependent gamma band amplitude was calculated from the time-frequency distribution for two gamma bands (40-80 Hz and 80-120 Hz). Among the two bands, the one that had the larger maximal z-score was used in the subsequent analysis. The threshold for detection of gamma increase was set to 95% confidence interval after Bonferroni correction for multiple comparisons. The start and end of gamma activity were defined as the time points where the gamma band activity crossed the threshold. In order to examine whether the recorded gamma band activity was generated at the recording site, phase of S signal as referenced by D signal was measured at every peak of D signal. This analysis was carried out in the time region from the gamma start to the spindle START. The time region after the spindle START was excluded from the analysis to avoid possible interference by harmonics of spindles. The significance of result was assessed using the Rayleight statistic *R*.

Recording sites

After recordings, the monkeys were deeply anesthetized with pentobarbital sodium (more than 50 mg/kg administered intravenously) and perfused through the heart with 10% formaldehyde neutral buffer solution. The electrode tracks were identified and plotted on a standard brain map.

Results

Database

Total number of recording days was 95 days (Monkey MA, 25 days; MB, 19 days; MC, 51 days) and total number of recording sites was 88 (MA, 30; MB, 32; MC, 26) (Fig. 1A and C). Total length of sleep was 763.4 h (MA, 200.3 h; MB, 149.8 h; MC, 413.3 h) and the total length of each sleep stage was 133.8 h during N1 (MA, 31.6 h; MB, 28.7 h; MC, 73.5 h), 161.7 h during N2 (MA, 51.6 h; MB, 39.4 h; MC, 70.2 h), 171.4 h during N3 (MA, 37.6 h; MB, 30.2 h; MC, 103.6 h), 207.8 h during N4 (MA, 50.1 h; MB, 35.7 h; MC, 122.0 h), and 89.1 h during REM (MA, 29.4 h; MB, 15.8 h; MC, 44.0 h). The data in the monkey showed characteristic patterns in each sleep stage in a consistent manner with the patterns in the human polysomnography, including spindles, k-complexes, vertex sharp waves, slow waves, rapid eye movements, and EMG. The number of NREM-REM cycle was 7.9±2.1 (mean±SD) a night, (MA, 9.1±2.2; MB, 7.6±1.7; MC, 7.4±2.0).

General statistics of spindles

I found the total number of 183424 sleep spindles during N2-4 (N2, 48607; N3, 60718; N4, 74099). The mean spindle density per electrode was 1.9±1.3 min^{-1} during N2-4 (N2, 1.9±1.0 min^{-1}; N3, 2.0±1.3 min^{-1}; N4, 1.8±1.5 min^{-1}), and there was no significant difference in the density between sleep stages (one-way repeated measures ANOVA, F=0.47, df=2, p>0.6). Spindles were identified at 83 (MA, 28; MB, 30; MC, 25) of the total 88 recording sites, which were distributed in areas 46d, 46v, 9, 8a, 8b, 6, 5, 7, 32, and 24 as well as the primary motor (M1), the primary somatosensory (S1), and the supplementary motor areas (SMA) (Fig. 3C). The duration of spindles was

0.83±0.26 s (N2, 0.83±0.27 s; N3, 0.84±0.27 s; N4, 0.81±0.25 s).

Amplitude of spindles

The peak amplitude of spindles was 39±26 μV during N2, 33±23 μV during N3, and 31±23 μV during N4. The difference was statistically significant between N2 and N3, and between N3 and N4 (one-way repeated measures ANOVA, F=822, df=2, $p<10^{-300}$; Scheffe's test, $p<10^{-16}$). The averaged amplitude of spindles was 23±14 μV during N2, 20±13 μV during N3, and 19±13 μV during N4. The difference was statistically significant between N2 and N3, and between N3 and N4 (one-way repeated measures ANOVA, F=838, df=2, $p<10^{-300}$; Scheffe's test, $p<10^{-16}$).

Frequency of spindles

In order to certify that spindles were successfully detected, the mean spectrum during the interval between START and END and that of non-spindle periods during N2-4 were compared. A result in Monkey MA is shown in Fig. 3A. The former (red) showed a peak in the range of spindle band (12-20 Hz), while the latter (blue) showed no clear peak, giving an evidence for successful detection of spindles.

Frequency of individual spindle was measured and the distribution was shown as histograms for areas 8a (A8a), 1 (S1), and 24 (A24) in Monkey MA (Fig. 3B). The spindles in these recording sites are different from each other in the frequency distribution. The mean frequency in each channel was measured, and was mapped on the brain image (Fig. 3C). The result depicted a topographical distribution of frequency of spindles on the cortex. One-way ANOVA confirmed that the frequency is different between cortical areas (F=17.1, df=12, $p<3\times10^{-16}$). The fastest spindles (>15 Hz) were

distributed in the dorsolateral prefrontal cortex (areas 46 and 8a). The frequency in areas 46d and 46v was significantly higher than any other areas except for area 8a (Scheffe's test, $p<0.05$). Spindles of intermediate frequency (14-15 Hz) were seen in the centroparietal and medial prefrontal areas, and the slowest ones (<14 Hz) appeared in the mesial frontal areas (areas 32 and 24). The map also shows the spindle density (Fig. 3C). In Fig. 3D, the mean frequency and mean density are plotted for each area. The difference of density between cortical areas was statistically significant (one-way ANOVA, $F=11.6$, $df=12$, $p<3\times10^{-12}$). There was a significant positive linear correlation ($r=0.864$, $p<0.0002$) between the frequency and the density (Fig. 3E).

Concordant and non-concordant spindles

In the example raw data in Fig. 2A, spindles in different areas appeared sequentially within a short interval. In order to assess whether this happened by chance or not, cross-correlation of START pulses was calculated. In Fig. 4A, cross-correlation is plotted for area 8a vs. S1 and area 24 vs. S1. In both cases, a significant increase in cross-correlation was observed (area 8a vs. S1, $p<2\times10^{-66}$; area 24 vs. S1, $p<4\times10^{-22}$ after Bonferroni correction for multiple comparisons). Among 210 available pairs of recording sites, 170 pairs showed significant increase in cross-correlation. For the 170 significant pairs, the concordance index Q was calculated. The distribution of Q is displayed in a histogram (Fig. 4B). In 75% of pairs, Q was below 0.1, while the highest value was 0.48. For inter-areal comparison of Q, the mean Q for each areal pair was shown (Fig. 4C), and Q was displayed on the brain map (Fig. 4D). The higher rate ($Q>0.1$) was seen in several pairs between bilaterally symmetrical regions (areas 9-9 and S1-S1) and between nearby regions (for example, areas 46-9, 46-46, 9-9, 9-8, 8-8,

9-32, 9-SMA, 8-SMA, SMA-SMA, 5-S1, and S1-S1 in the same hemisphere). These results indicate that most spindles occurred independently, although there was a significant correlation between spindles in different regions.

Temporal order of spindles in different regions

In order to examine temporal relationship between spindles in different regions, I measured time lags of the peak in the cross-correlogram across all the available pairs. For example, in the pair between area 8a and S1, the time lag was −0.12 s, while it was 0.64 s between area 24 and S1. The results were compiled and mapped on the brain image as relative values to the spindles in the right S1 (Fig. 5). One-way ANOVA revealed a significant difference in the time lag between cortical areas (F=14.6, df=12, $p<4\times10^{-14}$). In the medial frontoparietal cortex, the mean time lags in areas 8b, 24, and 32 were 0.33 s, 0.38 s, and 0.53 s, respectively, and the difference as compared to that in S1 was statistically significant (Scheffe's test, $p<0.05$). In contrast, in most areas in the dorsolateral frontoparietal cortex (areas 46, 9, 8a, 6, 5, and 7 and M1), the mean time lag in each area was within the range [−0.02 s, 0.13 s], and the difference as compared to that in S1 was not statistically significant (Scheffe's test, $p>0.05$). The result shows that spindles in the medial part are delayed as compared to those in the lateral part.

Frequency interaction of concurrent spindles

The above results indicate that spindles of different mean frequencies can occur concordantly. Consequently, the question arises whether the frequency of spindles in each area is modulated when they occur concurrently with spindles in other area. Frequency interaction of spindles was examined across the pairs of recording sites by

three criteria: 1) frequency difference of non-concurrent spindles in two regions was significant or not; 2) in ANOVA, the effect of concurrency on the frequency is significant or not; 3) the frequencies of a concurrent pair of spindles were linearly correlated or not. For convenience, the three criteria are denoted as FD (frequency difference), FS (frequency shift), and FC (frequency correlation), respectively, and '+/−' stands for 'significant/non-significant'. FD classifies the property of non-concurrent spindles, and FS+ and FC+ indicate the existence of significant interaction between the frequencies of concurrent spindles.

The total 210 pairs were classified into six different patterns as follows; (a) [FD−, FS−, FC−] (72 pairs), (b) [FD+, FS−, FC−] (107 pairs), (c) [FD+, FS+, FC−] (3 pairs), (d) [FD−, FS−, FC+] (11 pairs), (e) [FD+, FS−, FC+] (11 pairs), and (f) [FD+, FS+, FC+] (6 pairs). Theoretically, two more patterns can be supposed; (g) [FD−, FS+, FC−] and (h) [FD−, FS+, FC+]. However these two patterns were not detected. An example for each pattern is shown in Fig. 6A(a)-(f), and the cumulative result is displayed on the brain map (Fig. 6B). Patterns (a) and (b) are the cases with no significant interaction, while patterns (c), (d), (e), and (f) are the cases with significant interaction. Thus, no significant interaction was found in 179 pairs, while a significant interaction between concurrent spindles was found in the rest 31 pairs. The pairs of significant interaction were seen in several pairs between bilaterally symmetrical regions (areas 9-9 and S1-S1) and between nearby regions (for example, areas 46-9, 46-46, 9-9, 9-8, 9-32, 6-24, 9-SMA, 6-SMA, 8-SMA, SMA-SMA, 5-S1, 7-S1, M1-S1, and S1-S1 in the same hemisphere). In the patterns of (b), (c), (e), and (f) with [FD+], the frequency difference between concurrent spindles in two regions was also statistically significant. This result indicates that spindles of different frequencies

concurrently took place in these patterns. In the patterns of (d), (e), and (f) with [FC+], the correlation coefficient was always positive in all the 28 pairs, indicating a positive linear correlation. In the patterns of (c) and (f) with [FD+, FS+], the difference of mean frequency between two areas was narrower in the concurrent spindles than in the non-concurrent spindles in 7 of the total 9 pairs.

Cross-frequency coupling between spindles and slow waves

In Fig. 2A, two spindles in area 8a ride on approximately the same phase of the slow waves (orange line) extracted by a band-pass filter (0.1-1 Hz). In order to investigate whether spindles are related to slow potential shifts, I averaged raw data at the timing of START. Example results are shown for area 8a, S1, and area 24 in Monkey MA (Fig. 7A). Slow waves that have a period of more than 1 s can be seen around the START. Essentially the same effects were observed in various recording sites (data not shown). That indicates that spindles were superimposed on slow component (< 1Hz). The polarity of slow component was dependent on the area.

Then, the phase angle of slow waves (0.1-1 Hz) at START of spindles was measured. Example results are shown in Fig. 7B for the same recording sites as in Fig. 7A. They were shown as circular histograms, in which 0 degrees indicated the negative peak and 180 degrees the positive (see Fig. 7C). The mean phase angle for these examples was 182 degrees, 32 degrees, and 325 degrees, respectively, and the phase locking was statistically significant in all the three (N=642, R=0.35, $p<2\times10^{-36}$; N=1601, R=0.44, $p<3\times10^{-139}$; N=173, R=0.60, $p<3\times10^{-30}$). The mean phase angle was calculated for all cortical spindle sources, and was shown on the brain map (Fig. 7D).The phase locking was statistically significant in 58 sites of the total 83 cortical spindle sources

($p<0.05$ after Bonferroni correction for multiple comparisons). The result shows that spindles in the lateral anterior tended to start on the positive phase of slow waves, while spindles in the centroparietal and the mesial frontal areas were inclined to occur on the negative phase.

Phase relationship between slow waves

In order to examine the phase relationship of slow waves versus slow waves in various cortical areas, the phase angle of slow waves (0.1-1 Hz) was measured as referenced to the slow waves in the right S1. Only the data recorded simultaneously with the reference channel in S1 were used in this analysis. The example results obtained from area 5 and 8a in Monkey MA are shown in Fig. 8A. The mean phase angle for these examples was 34 degrees and 206 degrees, respectively, and the phase locking was statistically significant in both sites (N=6353, R=0.57, $p<10^{-300}$; N=1960, R=0.29, $p<3\times10^{-75}$). The cumulative result was shown on the brain image (Fig. 8B). The phase locking was statistically significant in 35 sites of the total 37 available recording sites ($p<0.05$ after Bonferroni correction for multiple comparisons). The result indicates that phase angle of slow waves is reversed between the central region and the prefrontal region. The boundary seems to be between M1 and area 6. In addition, the phase angle seems to be reversed between the central region and area 7, although the number of data points is small.

Cross-frequency coupling between spindles and gamma oscillations

In the time-frequency distribution of a single spindle (Fig. 2E), gamma activity (40-120 Hz) is seen before START in parallel with 1-5 Hz activity reflecting the

k-complex and slow waves below 1 Hz. In order to examine the detailed property of gamma activity around spindles, the time-frequency distribution was averaged separately at the timings of STARTs and PEAKs of spindles, and the resulted maps were normalized to z-score. Example results are shown for area 8a and S1 in Monkey MA (Fig. 9A). The upper row shows maps aligned at START, and the lower shows ones aligned at PEAK. Both in area 8a and S1, gamma activity was significantly increased before START, and the increase lasted to about the time point of PEAK. There can be seen also slow waves (<1 Hz) and 1-5 Hz activity that presumably corresponds to k-complexes around the spindle.

The mean gamma phase difference between S and D was in anti-phase (179 degrees and 179 degrees for area 8a and S1, respectively), and the phase locking was statistically significant (N=1185, R=0.28, $p<3\times10^{-42}$; N=2360, R=0.66, $p<10^{-300}$, respectively) (Fig. 9B). The result indicates that these gamma activities were probably generated at the recorded sites.

Recording sites were identified as significant gamma generators, when both the gamma increase and phase reversal were statistically significant. The distribution of significant gamma activity was plotted with filled marks in Fig. 9C. The color of the marks denotes the onset time of gamma activity as measured from spindle START in each recording site. Among 83 cortical spindle sources, 40 sites were identified as significant gamma generators. They were found in areas 9, 46, and 8 in three monkeys, areas 6 and 7 in Monkey MA, area 32 and SMA in Monkey MC, and S1 in Monkeys MA and MC. The timing of gamma onset was −0.29±0.14 s. When the timing of gamma onset measured from the START of S1 spindle was estimated using the intercortical spindle time lags determined in Fig. 5, it was −0.20±0.11 s. The latter deviation (0.11 s)

was smaller than the former (0.14 s), although the difference was not statistically significant (F-test, $p>0.09$). The mean duration of gamma increase was 0.49±0.28 s. The timing of gamma end was 0.19±0.25 s as measured from spindle START, and −0.13±0.25 s as measured from spindle PEAK. The results indicate that short bursts of gamma oscillations emerged before the spindle START and lasted to about the spindle PEAK.

Discussion

Similarity between humans and monkeys

Regarding the characteristic short bursts of 12-20 Hz rhythmic waves during sleep in the cortical field potentials of the monkey, I propose that the activity is equivalent to the sleep spindles in the human by the following homologies. 1) The frequency is similar between the human sleep spindles and the monkey counterpart. In the present study, the individual spindle in the monkey was collected in the range of 12-20 Hz, and the mean frequency in each recording site distributed between 13-17 Hz. Although this range is slightly higher than that of the human spindles (11-16 Hz) (Nakamura et al. 2003; Silber et al. 2007; Werth et al. 1997; Zeitlhofer et al. 1997; Zygierewicz et al. 1999), the difference may be attributable to species difference between the monkey and the human. 2) The duration (0.83±0.26 s) is comparable to that reported in the human (0.5-1.2 s) (Nicolas et al. 2001; Zeitlhofer et al. 1997). 3) The mean spindle density per electrode (1.9 min^{-1}) is in accordance with the value reported in intracranial recordings in the human (1.8 min^{-1} in frontal lobe; 1.3 min^{-1} in parietal lobe) (Andrillon et al. 2011). 4) The NREM-REM modulation of spindles and other patterns such as k-complexes, vertex sharp waves, slow waves, EOG, and EMG seems similar to those in the human. The number of cycles (7.9±2.1) per night in the present study overlaps with 4-6 cycles in the human (Kandel 2000; Le Bon et al. 2002; Preud'homme et al. 2000).

According to the above similarities, the spindles in the monkey may be useful as a functional model of the human sleep spindles.

Localization of cortical current generators of spindles

In human EEG, sleep spindles are most frequently recorded over the central head regions (McCormick et al. 1997). The source regions were estimated in the dorsolateral and medial frontal cortex and parietal cortex (Anderer et al. 2001; Ishii et al. 2003; Manshanden et al. 2002; Schabus et al. 2007). The present study confirmed the current generators of spindles in wide cortical regions including the prefrontal, centroparietal, and mesial frontal cortices using direct recording with transcortical electrode pairs (Fig. 3C). It seems that virtually all cortical areas can generate spindles, because no cortical area was specifically determined as a spindle-free area so far.

Frequency of spindles

In the human, it has been recognized that the frequency of centroparietal spindles is higher and that of frontal spindles is lower (Jankel and Niedermeyer 1985). The present study revealed that each cortical source generated spindles around a particular frequency for each source (Fig. 3C). However, the topographic pattern of the frequency in the monkey was different to the human in that the frequency of the monkey was higher in the prefrontal region than in the centroparietal. The reason for this difference is unknown. More developed prefrontal cortex or larger dimension in the human brain may cause the difference.

In addition, a significant positive correlation between spindle frequency and the spindle density was found (Fig. 3E). That suggests a close relationship between the rhythm generator and the triggering system of spindles. The previous studies in cats under ketamine/xylazine anesthesia suggested that the recurrent inhibitory loop between the thalamic reticular nucleus (TRN) neurons and thalamo-cortical neurons may play an important role in the generation of the spindle rhythm (Steriade et al. 1990). The

properties of thalamocortical neurons such as membrane potential might be reflected on both the rhythm and spindle density.

Concordant and non-concordant spindles

In the human, it is reported that the majority of spindles take place independently in local cortical regions, while relatively small number of spindles occur concomitantly across multiple regions (Andrillon et al. 2011; Nir et al. 2011). The present study revealed that spindles have significant tendency to occur concordantly in different recording sites, although the concordance rate is relatively low in most of pairs of the recording sites (Fig. 4B). That is in good accordance with the human results. Furthermore, the present result showed that the concordance rate was relatively high in some of the pairs between bilaterally symmetrical regions and between nearby regions (Fig. 4CD). These combinations overlap to the cortical regions which have corticocortical connections via the commissural fibers and the short association fibers (U-fibers) (Iwamura 2000; Jones and Hendry 1980; Karol and Pandya 1971; Morris et al. 1999). The corticocortical links may play an important role in the synchronized initiation of spindles. Crossed thalamocortical and corticothalamic projections (Molinari et al. 1985; Preuss and Goldman-Rakic 1987) and crossed projections from the TRN to the thalamus (Raos and Bentivoglio 1993; Rinvik 1984) may also contribute to the bilateral synchronization to some extent.

Temporal organization of spindles

In human studies, it is reported that fast spindles in the centroparietal cortex tend to precede slow ones in the anterior with a time lag of about 0.2-0.5 s (Andrillon et

al. 2011; Mölle et al. 2011). The present study revealed a detailed temporal organization of the spindle generation that spindles tend to occur sequentially in a lateral-medial order (Fig. 5). The time lag from the lateral to the mesial was approximately 0.5 s. There was a tendency that fast spindles precede slow ones also in the monkey. However, no significant difference in the timing was noted between the prefrontal area 46 and S1, although spindles in these areas had different frequencies. Therefore, the time lag may be better interpreted as a correlate of laterality than as a correlate of frequency.

Multiple rhythm generators of spindles

It has been a matter of debate whether the oscillations of fast and slow spindles are derived from independent rhythm sources or simply the result of modulation of a single rhythm generator (De Gennaro and Ferrara 2003; Mascetti et al. 2011; Rasch and Born 2013). The present results indicated that spindles of different frequencies can simultaneously take place ([FD+] in Fig. 6). That suggests the existence of multiple rhythm generators of spindles. This is in accordance with human studies using magnetoencephalography, low-resolution brain electromagnetic tomography, or intracranial electrodes (Anderer et al. 2001; Andrillon et al. 2011; Dehghani et al. 2010). As spindle rhythms are assumed to be generated by circuits including the thalamus and TRN (Steriade et al. 1990), multiple rhythm generators may coexist for different cortical regions. This is because the projections between the cortex and TRN and between the cortex and thalamus are segregated between cortical regions in a topographic manner (Guillery et al. 1998; Jones et al. 1979; Rouiller and Welker 2000; Schell and Strick 1984; Zikopoulos and Barbas 2006).

In the majority of the recording sites, the frequency was not affected by other spindles concurrently occurred in other regions ([FS−, FC−] in Fig. 6). The results suggest that each rhythm generator is mostly independent from other generators. However, in several combinations of the recording sites, significant interactions between two rhythms were observed. I found two types of interactions. One is the shift of frequency distribution mostly in the direction to lessen the frequency difference ([FS+] in Fig. 6). The other is the positive linear correlation of frequency between two regions ([FC+] in Fig. 6). These interactions were noted in some of the combination between bilaterally symmetrical regions and between nearby regions. The pairs were overlapped with the pairs with higher concordance index *Q*. In these pairs, the corticocortical connections and the crossed projections between the thalamus and the cortex or TRN may cause entrainment of oscillations.

Correlation between spindles and slow waves

The present study showed that spindles in each cortical region occurred preferentially around a particular phase of slow waves at the recording sites (Fig. 7). In the dorsolateral prefrontal cortex, spindles occurred around the positive phase of slow waves, while, in the centroparietal cortex, spindles appeared around the negative phase. Because the dorsolateral prefrontal cortex produces the faster spindles and the centroparietal cortex generates the slower ones, this result is in good accordance with the human result that fast spindles ride on the positive phase of slow waves, while slow spindles ride on the negative phase(Mölle et al. 2011; Mölle et al. 2002).

In addition, the present study revealed a phase relationship among slow waves in different regions (Fig. 8). There is a tendency that phase of slow waves is reversed

between the prefrontal cortex and the sensorimotor cortex. The phase at the posterior to the intraparietal sulcus is also reversed as compared to the sensorimotor cortex, although more number of recording sites may be required for confirmation. This phase relationship may explain the reason why fast spindles and slow spindles ride on the opposite phases of slow waves. As shown in the present study, spindles in various sites have tendency to take place sequentially within a time lag of 0.5 s, while slow waves themselves have phase relations. Consequently, spindles in the prefrontal and the sensorimotor cortices are observed on the opposite phases of slow waves.

K-complexes may partly contribute to the correlation between slow waves and spindles, because they often precede spindles predominantly in frontal regions (for example, Fig. 2A) and contain slow components (<1 Hz) as well as delta band (1-4 Hz) activity (Amzica and Steriade 1997; Colrain 2005; Happe et al. 2002; McCormick et al. 1997).

Recent observations in the human have shown that slow waves during SWS can be regulated locally (Nir et al. 2011) and can propagate over the cortex as a travelling wave (Massimini et al. 2004). In contrast, the present results suggest a global regulation of slow waves. Although the reason for this difference is unknown, it may be caused by the difference in the brain size between humans and monkeys.

Correlation between spindles and gamma oscillations

The present study revealed that an increase in the amplitude of gamma oscillations preceded the START of spindles with a time lag of 0.29±0.14 s (Fig. 9). The increased gamma activity lasted about 0.5 s, and then decreased around the time point of peak amplitude of spindles. When the gamma activities are aligned at the

START of S1 spindle using the intercortical spindle time lags determined in Fig. 5, the time lags of gamma onset become 0.20±0.11 s. Because the deviation measured from the S1 START is smaller than the deviation measured from the START in each recording site, it may be better to say that the gamma increase is globally time locked together than to say that it is locked to spindle onset in each recording site.

The gamma increase before the spindle has not been reported to our knowledge. In human epileptic patients, it is reported that cortical gamma oscillations during NREM sleep emerge preferentially on a certain phase of slow waves synchronously in many different cortical areas (Le Van Quyen et al. 2010; Valderrama et al. 2012). Gamma activity coupled with spindle is reported in the human (Ayoub et al. 2012). They seem partially in accordance with the feature of gamma activity found in the present study.

Functional significance

The present study showed that spindles in different regions are driven by their own rhythm sources, nevertheless they are temporally and spatially related with each other, and that they are correlated with slow waves and gamma oscillations. Such interactions may serve as a functional basis to transfer information in large-scale brain network during memory consolidation (Canolty and Knight 2010). Although detailed explanation of the neural mechanism for these correlations is beyond the scope of the present study, a possible mechanism has been proposed by Steriade (Steriade 2006). According to the theory, cortically generated slow oscillation is effective in integrating different rhythms including spindles and gamma rhythms through corticocortical and corticothalamic drives.

Because the prominent inter-spindle correlations were found between the bilaterally symmetrical regions and between the nearby regions, corticocortical connections and crossed projections between the thalamus and the cortex or TRN may play a significant role in the spatiotemporal correlations of spindles. The cross-frequency couplings suggest that the triggering system for spindles is linked with slow waves and gamma oscillations. Because the gamma increase is limited within a short time region around the spindle START, they may serve as a direct trigger of spindles. However, it is unexplained that some cortical spindle sources showed no significant gamma increase. Causal relationship between the gamma activity and spindle should be further investigated.

Conclusion

The present study revealed a constellation of correlations between spindles and slow and gamma oscillations in the monkey. They may be a clue to understanding the mechanism for information processing during SWS.

References

Amzica F, and Steriade M. The K-complex: its slow (<1-Hz) rhythmicity and relation to delta waves. *Neurology* 49: 952-959, 1997.

Anderer P, Klösch G, Gruber G, Trenker E, Pascual-Marqui R, Zeitlhofer J, Barbanoj M, Rappelsberger P, and Saletu B. Low-resolution brain electromagnetic tomography revealed simultaneously active frontal and parietal sleep spindle sources in the human cortex. *Neuroscience* 103: 581-592, 2001.

Andrillon T, Nir Y, Staba RJ, Ferrarelli F, Cirelli C, Tononi G, and Fried I. Sleep Spindles in Humans: Insights from Intracranial EEG and Unit Recordings. *J Neurosci* 31: 17821-17834, 2011.

Ayoub A, Mölle M, Preissl H, and Born J. Grouping of MEG gamma oscillations by EEG sleep spindles. *NeuroImage* 59: 1491-1500, 2012.

Buzsáki G, and Wang XJ. Mechanisms of gamma oscillations. *Annu Rev Neurosci* 35: 203-225, 2012.

Canolty RT, and Knight RT. The functional role of cross-frequency coupling. *Trends Cogn Sci* 14: 506-515, 2010.

Colrain IM. The K-complex: a 7-decade history. *Sleep* 28: 255-273, 2005.

Cox R, Hofman WF, and Talamini LM. Involvement of spindles in memory consolidation is slow wave sleep-specific. *Learn Mem* 19: 264-267, 2012.

De Gennaro L, and Ferrara M. Sleep spindles: an overview. *Sleep Med Rev* 7: 423-440, 2003.

Dehghani N, Cash SS, Rossetti AO, Chen CC, and Halgren E. Magnetoencephalography demonstrates multiple asynchronous generators during human sleep spindles. *J Neurophysiol* 104: 179-188, 2010.

Diekelmann S, and Born J. The memory function of sleep. *Nat Rev Neurosci* 11: 114-126, 2010.

Eschenko O, Mölle M, Born J, and Sara SJ. Elevated sleep spindle density after learning or after retrieval in rats. *J Neurosci* 26: 12914-12920, 2006.

Fogel SM, and Smith CT. The function of the sleep spindle: a physiological index of intelligence and a mechanism for sleep-dependent memory consolidation. *Neurosci Biobehav Rev* 35: 1154-1165, 2011.

Gais S, Mölle M, Helms K, and Born J. Learning-dependent increases in sleep spindle density. *J Neurosci* 22: 6830-6834, 2002.

Gross DW, and Gotman J. Correlation of high-frequency oscillations with the sleep-wake cycle and cognitive activity in humans. *Neuroscience* 94: 1005-1018, 1999.

Guillery R, Feig S, and Lozsadi D. Paying attention to the thalamic reticular nucleus. *Trends neurosci* 21: 28-32, 1998.

Happe S, Anderer P, Gruber G, Klosch G, Saletu B, and Zeitlhofer J. Scalp topography of the spontaneous K-complex and of delta-waves in human sleep. *Brain Topogr* 15: 43-49, 2002.

Huang NE. Introduction to the Hilbert-Huang transfrom and its related mathematical problems. In: *Hilbert-Huang transform and its applications*, edited by Huang NE, and Shen SS. New Jersey: World Scientific, 2005, p. 1-26.

Huang NE, Shen Z, Long SR, Wu MC, Shih HH, Zheng Q, Yen N-C, Tung CC, and Liu HH. The empirical mode decomposition and the Hilbert spectrum for nonlinear and non-stationary time series analysis. *Proc R Soc A* 454: 903-995, 1998.

Ishii R, Dziewas R, Chau W, Soros P, Okamoto H, Gunji A, and Pantev C. Current

source density distribution of sleep spindles in humans as found by synthetic aperture magnetometry. *Neurosci Lett* 340: 25-28, 2003.

Iwamura Y. Bilateral receptive field neurons and callosal connections in the somatosensory cortex. *Philos Trans R Soc Lond B Biol Sci* 355: 267-273, 2000.

Jankel W, and Niedermeyer E. Sleep spindles. *J Clin Neurophysiol* 2: 1, 1985.

Jobert M, Poiseau E, Jahnig P, Schulz H, and Kubicki S. Topographical analysis of sleep spindle activity. *Neuropsychobiology* 26: 210-217, 1992.

Jones E, and Hendry S. Distribution of callosal fibers around the hand representations in monkey somatic sensory cortex. *Neurosci Lett* 19: 167-172, 1980.

Jones EG, Wise SP, and Coulter JD. Differential thalamic relationships of sensory-motor and parietal cortical fields in monkeys. *J Comp Neurol* 183: 833-881, 1979.

Kandel ERS, J H.; Jessell, T M. *PRINCIPLES OF NEURAL SCIENCE*. New York: McGraw-Hill Health Professions Division, 2000, p. 1414 pages.

Karol EA, and Pandya DN. The distribution of the corpus callosum in the Rhesus monkey. *Brain* 94: 471-486, 1971.

Le Bon O, Staner L, Rivelli SK, Hoffmann G, Pelc I, and Linkowski P. Correlations using the NREM-REM sleep cycle frequency support distinct regulation mechanisms for REM and NREM sleep. *J Appl Physiol (1985)* 93: 141-146, 2002.

Le Van Quyen M, Staba R, Bragin A, Dickson C, Valderrama M, Fried I, and Engel J. Large-Scale Microelectrode Recordings of High-Frequency Gamma Oscillations in Human Cortex during Sleep. *J Neurosci* 30: 7770, 2010.

Logothetis NK, Eschenko O, Murayama Y, Augath M, Steudel T, Evrard H, Besserve M, and Oeltermann A. Hippocampal-cortical interaction during periods

of subcortical silence. *Nature* 491: 547-553, 2012.

Loomis AL, Harvey EN, and Hobart G. Potential Rhythms of the Cerebral Cortex during Sleep. *Science* 81: 597-598, 1935.

Lord Rayleigh. On the resultant of a large number of vibrations of the same pitch and of arbitrary phase. *Philos Mag* 10: 73-78, 1880.

Mölle M, Bergmann TO, Marshall L, and Born J. Fast and slow spindles during the sleep slow oscillation: disparate coalescence and engagement in memory processing. *Sleep* 34: 1411-1421, 2011.

Mölle M, Marshall L, Gais S, and Born J. Grouping of spindle activity during slow oscillations in human non-rapid eye movement sleep. *J Neurosci* 22: 10941-10947, 2002.

Manshanden I, De Munck JC, Simon NR, and Lopes da Silva FH. Source localization of MEG sleep spindles and the relation to sources of alpha band rhythms. *Clin Neurophysiol* 113: 1937-1947, 2002.

Mascetti L, Foret A, Shaffii-Le Bourdiec A, Muto V, Kussé C, Jaspar M, Matarazzo L, Dang-Vu T, Schabus M, and Maquet P. Spontaneous neural activity during human non-rapid eye movement sleep. *Prog Brain Res* 193: 111, 2011.

Massimini M, Huber R, Ferrarelli F, Hill S, and Tononi G. The sleep slow oscillation as a traveling wave. *J Neurosci* 24: 6862-6870, 2004.

McCormick L, Nielsen T, Nicolas A, Ptito M, and Montplaisir J. Topographical distribution of spindles and K-complexes in normal subjects. *Sleep* 20: 939-941, 1997.

Molinari M, Minciacchi D, Bentivoglio M, and Macchi G. Efferent fibers from the

motor cortex terminate bilaterally in the thalamus of rats and cats. *Exp Brain Res* 57: 305-312, 1985.

Morris R, Pandya DN, and Petrides M. Fiber system linking the mid-dorsolateral frontal cortex with the retrosplenial/presubicular region in the rhesus monkey. *J Comp Neurol* 407: 183-192, 1999.

Nakamura M, Uchida S, Maehara T, Kawai K, Hirai N, Nakabayashi T, Arakaki H, Okubo Y, Nishikawa T, and Shimizu H. Sleep spindles in human prefrontal cortex: an electrocorticographic study. *Neurosci Res* 45: 419-427, 2003.

Ngo HV, Martinetz T, Born J, and Molle M. Auditory Closed-Loop Stimulation of the Sleep Slow Oscillation Enhances Memory. *Neuron* 2013.

Nicolas A, Petit D, Rompre S, and Montplaisir J. Sleep spindle characteristics in healthy subjects of different age groups. *Clin Neurophysiol* 112: 521-527, 2001.

Nir Y, Staba RJ, Andrillon T, Vyazovskiy VV, Cirelli C, Fried I, and Tononi G. Regional slow waves and spindles in human sleep. *Neuron* 70: 153-169, 2011.

Peigneux P, Laureys S, Delbeuck X, and Maquet P. Sleeping brain, learning brain. The role of sleep for memory systems. *Neuroreport* 12: A111-A124, 2001.

Preud'homme XA, Lanquart JP, Mendlewicz J, and Linkowski P. Characteristics of spontaneous sleep with varying NREMS Episodes in healthy men: implication for delta activity homeostasis. *Sleep* 23: 193-203, 2000.

Preuss TM, and Goldman-Rakic PS. Crossed corticothalamic and thalamocortical connections of macaque prefrontal cortex. *J Comp Neurol* 257: 269-281, 1987.

Raos V, and Bentivoglio M. Crosstalk between the two sides of the thalamus through the reticular nucleus: a retrograde and anterograde tracing study in the rat. *J Comp Neurol* 332: 145-154, 1993.

Rasch B, and Born J. About sleep's role in memory. *Physiol Rev* 93: 681-766, 2013.

Rechtschaffen A, and Kales A. *A manual of standardized terminology, techniques and scoring system for sleep stages of human subjects*. Washington, DC: Washington Public Health Service, US Government Printing Office, 1968.

Rinvik E. Thalamic commissural connections in the cat. *Neurosci Lett* 44: 311-316, 1984.

Rouiller EM, and Welker E. A comparative analysis of the morphology of corticothalamic projections in mammals. *Brain Res Bull* 53: 727-741, 2000.

Schabus M, Dang-Vu TT, Albouy G, Balteau E, Boly M, Carrier J, Darsaud A, Degueldre C, Desseilles M, Gais S, Phillips C, Rauchs G, Schnakers C, Sterpenich V, Vandewalle G, Luxen A, and Maquet P. Hemodynamic cerebral correlates of sleep spindles during human non-rapid eye movement sleep. *Proc Natl Acad Sci U S A* 104: 13164-13169, 2007.

Schabus M, Hodlmoser K, Gruber G, Sauter C, Anderer P, Klosch G, Parapatics S, Saletu B, Klimesch W, and Zeitlhofer J. Sleep spindle-related activity in the human EEG and its relation to general cognitive and learning abilities. *Eur J Neurosci* 23: 1738-1746, 2006.

Schell GR, and Strick PL. The origin of thalamic inputs to the arcuate premotor and supplementary motor areas. *J Neurosci* 4: 539-560, 1984.

Silber M, Ancoli-Israel S, Bonnet M, Chokroverty S, Grigg-Damberger M, Hirshkowitz M, Kapen S, Keenan S, Kryger M, and Penzel T. The visual scoring of sleep in adults. *J Clin Sleep Med* 3: 121-131, 2007.

Sirota A, Csicsvari J, Buhl D, and Buzsáki G. Communication between neocortex and hippocampus during sleep in rodents. *Proc Natl Acad* 100: 2065, 2003.

Squire LR. Memory and the hippocampus: a synthesis from findings with rats, monkeys, and humans. *Psychol Rev* 99: 195-231, 1992.

Steriade M. Grouping of brain rhythms in corticothalamic systems. *Neuroscience* 137: 1087-1106, 2006.

Steriade M, Gloor P, Llinas R, Lopes da Silva F, and Mesulam M. Basic mechanisms of cerebral rhythmic activities. *Electroencephalogr Clin Neurophysiol* 76: 481 508, 1990.

Takeuchi S, Mima T, Murai R, Shimazu H, Isomura Y, and Tsujimoto T. Gamma oscillations and their cross-frequency coupling in the primate hippocampus during sleep. *Sleep* in press, 2015.

Valderrama M, Crepon B, Botella-Soler V, Martinerie J, Hasboun D, Alvarado-Rojas C, Baulac M, Adam C, Navarro V, and Le Van Quyen M. Human gamma oscillations during slow wave sleep. *PLoS One* 7: e33477, 2012.

Wang X-J. Neurophysiological and computational principles of cortical rhythms in cognition. *Physiol Rev* 90: 1195-1268, 2010.

Werth E, Achermann P, Dijk DJ, and Borbély AA. Spindle frequency activity in the sleep EEG: individual differences and topographical distribution. *Electroen Clin Neuro* 103: 535-542, 1997.

Zeitlhofer J, Gruber G, Anderer P, Asenbaum S, Schimicek P, and Saletu B. Topographic distribution of sleep spindles in young healthy subjects. *J Sleep Res* 6: 149-155, 1997.

Zikopoulos B, and Barbas H. Prefrontal projections to the thalamic reticular nucleus form a unique circuit for attentional mechanisms. *J Neurosci* 26: 7348, 2006.

Zygierewicz J, Blinowska KJ, Durka PJ, Szelenberger W, Niemcewicz S, and

Androsiuk W. High resolution study of sleep spindles. *Clin Neurophysiol* 110: 2136-2147, 1999.

Figure legends

Figure 1. Arrangement of recording electrodes. (**A**) Symbols indicate the position of electrodes. Symbols placed adjacent to sulci stand for recording sites in the banks of sulci. (**B**) Schematic examples of the surface (S) and depth (D) electrodes. (**C**) The number of electrodes is shown for each area. Abbreviations: A, area; SMA, supplementary motor area; M1, primary motor area; S1, somatosensory area.

Figure 2. Automatic detection of spindles. (**A**) Segment of the raw waveform of S−D potentials recorded from A8a, S1, A6 and A24 in Monkey MA during stage N4 is shown. Pink and green circles indicate START and END of spindles automatically detected. Orange lines are band-pass filtered (<1 Hz) waveforms. (**B**) The first step of spindle detection. Raw data (black) were band-pass filtered (light blue) and the envelope was extracted (blue). Spindles were detected (red envelope) at the threshold of mean+3SD (red broken line) of the envelope. START (pink circle) and END (green circle) were determined by the mean+SD line (green broken line) (see text). (**C**) The second step of detection. Phase difference within the spindle band between S and D was measured at every peak of D (vertical lines). (**D**) For the exemplified spindle in **C**, the phase difference between S and D is displayed in a circular histogram. (**E**) The third step of detection. The spectral profile of spindle was examined on a time-frequency representation. The interval between START and END (pink and green vertical lines) were separated into 4 sections (a-d) and the marginal spectra were calculated for respective sections. (**F**) The marginal spectra were plotted. Note that all spectra have a peak within the spindle band (12-20 Hz: the interval between horizontal lines).

Figure 3. Frequency and density of spindles. (**A**) The mean spectra of spindles (red line) and that of non-spindle periods (blue line) in A8a in Monkey MA are shown. Logarithmic scale is used for frequency axis. (**B**) The frequency distributions of spindles in A8a, S1, and A24 in MA are shown. The positions of recording sites are shown in **C** with corresponding asterisk, dagger, and double-dagger. (**C**) The mean frequency and density of spindles are shown. Symbol color indicates frequency and the size stands for density. Open symbols stand for the sites with no significant spindles. (**D**) Red marks stand for spindle density, while blue marks show frequency in each area. The dots and bars represent mean and standard error of mean. (**E**) Correlation between the density and frequency of spindles are shown in an xy-plot.

Figure 4. Concordant and non-concordant spindles. (**A**) The cross-correlation of START pulses is shown for A8a vs. S1 and A24 vs. S1 in Monkey MA. The green and red lines are the mean and mean+2SD levels of randomly shuffled same data. The positions of recording sites are shown in **D** with corresponding asterisk, dagger, and double-dagger. (**B**) The distribution of concordance index *Q* is displayed in a histogram. (**C**) The mean *Q* is displayed for various areal pairs separately for contralateral and ipsilateral combinations. Open squares represent non-significant pairs, and grey ones mean no data were available. (**D**) The pairs with significant correlation are connected by colored lines. Black lines indicate non-significant pairs. Color scale is for **B**, **C**, and **D**.

Figure 5. Time lags of spindles. The relative time lags of spindle START as referenced to the spindle START in right S1 are shown. The bordered symbols in the right S1 indicate the reference channel in each monkey. Color shows time lag.

Figure 6. Frequency of concurrent spindles. (**A**) Frequency of spindles is compared between a pair of recording sites (red and light blue). Four histograms in a column show frequency of non-concurrent spindles (top and bottom) and concurrent spindles (second and third). Vertical blue lines stand for the mean frequency. The images below the histograms are xy-plots to explore the linear correlation between concurrent spindle pairs. The x and y axes correspond to the frequency in the second (light blue) and third (red) histograms, respectively. A Gaussian filter with a full width at half maximum of 0.7 Hz × 0.7 Hz was applied to the plots for presentation purposes only. The behavior of frequency was examined from the viewpoints of frequency difference (FD), frequency shift (FS), and frequency correlation (FC). By repeating the analysis across all the available pairs, each pair was classified into one of the six patterns of (a)-(f) (see Results). The positions of recording sites are shown in **B** with corresponding letters a-f. (**B**) The classification into the six patterns is displayed on the brain map.

Figure 7. Correlation between slow waves and spindles. (**A**) The averaged raw data at the timing of START in A8a, S1, and A24 in Monkey MA are shown. The positions of recording sites are shown in **D** with corresponding asterisk, dagger, and double-dagger. (**B**) The slow-wave phase at the timing of START in A8a, S1, and A24 in MA is shown. (**C**) The coordinate system of phase used in the present study is shown. (**D**) The mean slow-wave phase at the timing of START is displayed. The size of symbols indicates the degree of phase locking (Rayleigh statistic *R*). Open symbols denote that phase locking was not statistically significant.

Figure 8. Correlation between slow waves. (**A**) The slow-wave phases in A5 (left) and in A8a (right) as referenced to the phase in S1 in Monkey MA are shown. The positions of recording sites are shown in **B** with corresponding asterisk and dagger. (**B**) The mean slow-wave phase in each recording site is mapped on the brain image. The bordered symbols in the right S1 indicate the reference channel in each monkey. Open symbols denote that phase locking was not statistically significant.

Figure 9. Correlation between gamma oscillations and spindles (**A**) The mean normalized time-frequency distribution aligned at START (top) and PEAK (below) is shown for A8a and S1 in Monkey MA. Black contour lines represent the significance threshold at $p<0.05$ after Bonferroni correction. Note that the increase in the gamma band precedes START. The positions of recording sites are shown in **C** with corresponding asterisk and dagger. (**B**) The phase difference of gamma oscillations between S and D is shown. (**C**) The onset time of gamma increase as measured from START in each recording site is shown. Open symbols mean that no significant gamma activity was identified. The mean onset time was -0.29 ± 0.14 s.

Figure 1

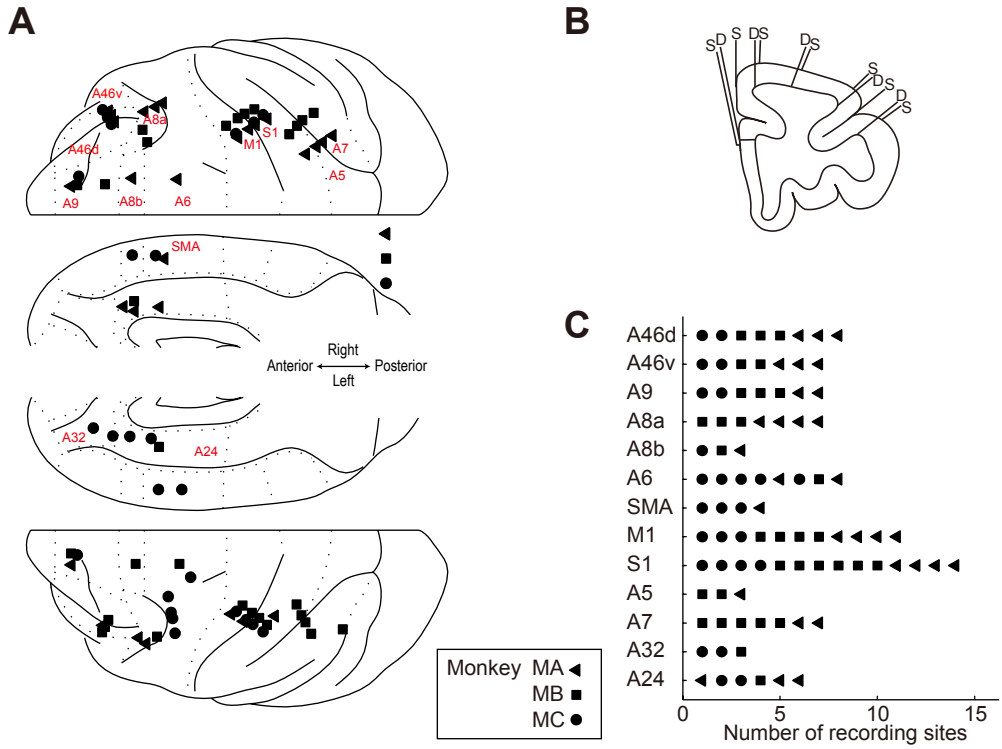
A
A46v
A8a
A46d
M1
S1
A7
A5
A9
A8b
A6
SMA
Right
Anterior
Posterior
Left
A32
A24
Monkey MA
MB
MC
B
SD S DS Ds S DS D S
C
A46d
A46v
A9
A8a
A8b
A6
SMA
M1
S1
A5
A7
A32
A24
0 5 10 15
Number of recording sites

Figure 2

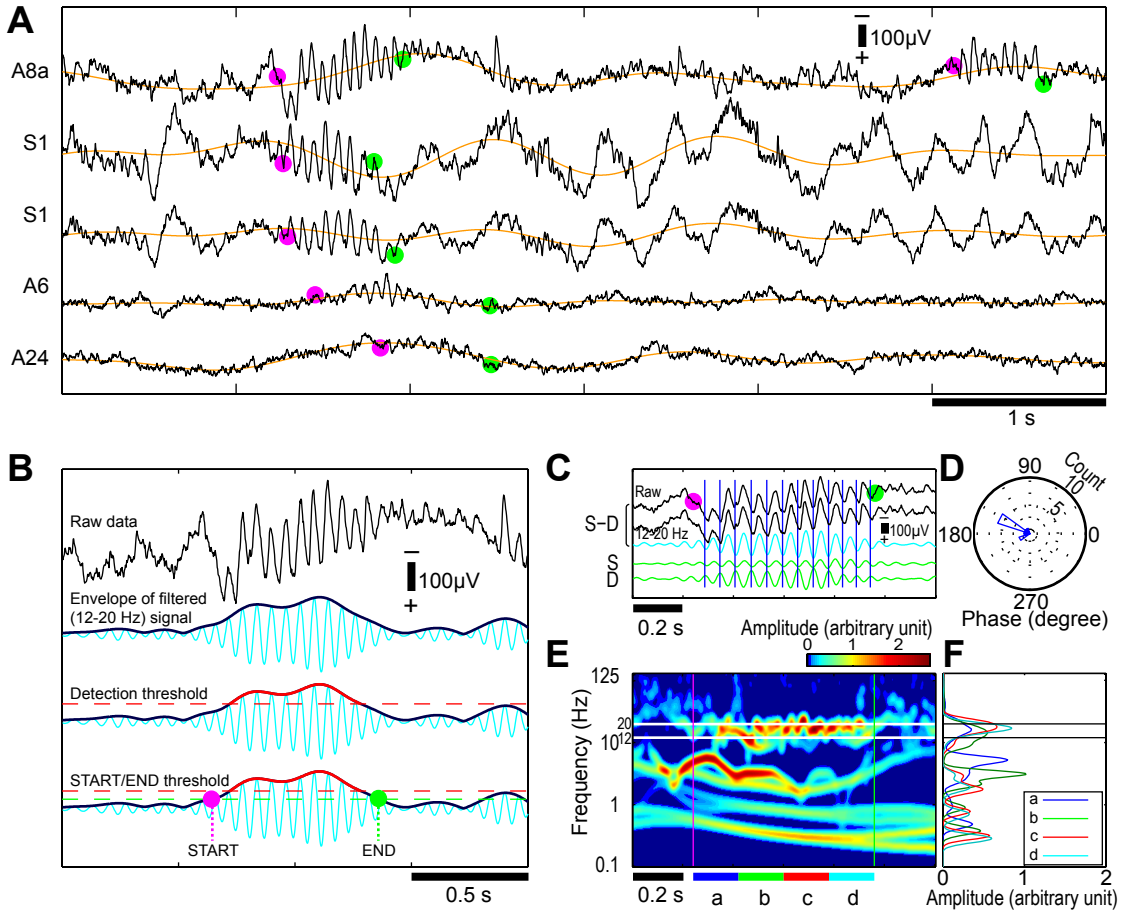
A
A8a
S1
S1
A6
A24
100μV
1 s
B
Raw data
Envelope of filtered
(12-20 Hz) signal
Detection threshold
START/END threshold
START
END
100μV
0.5 s
C
Raw
S-D
12-20 Hz
S
D
100μV
0.2 s
Amplitude (arbitrary unit)
D
90
Count
10
5
180
0
270
Phase (degree)
E
125
20
10
12
1
0.1
Frequency (Hz)
0.2 s
a
b
c
d
F
0
1
2
Amplitude (arbitrary unit)
a
b
c
d

Figure 3

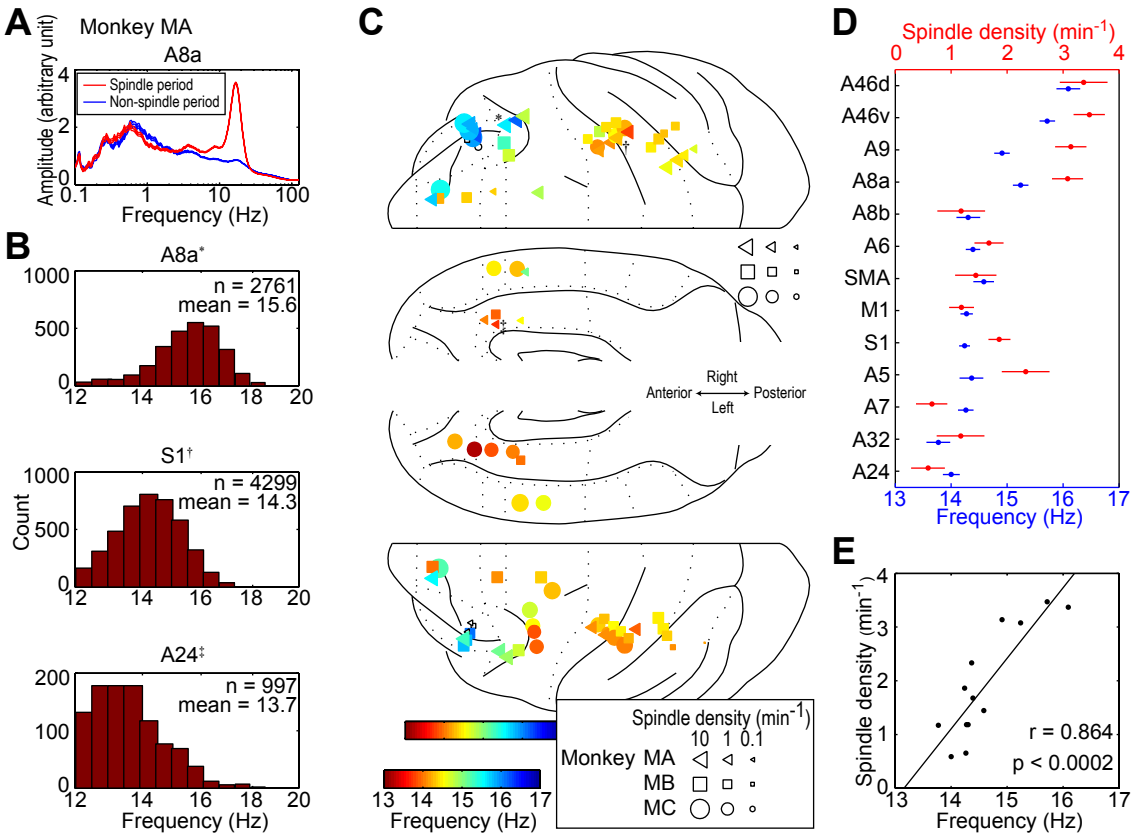
A
Monkey MA
A8a
Spindle period
Non-spindle period
Amplitude (arbitrary unit)
Frequency (Hz)
B
A8a*
n = 2761
mean = 15.6
S1†
n = 4299
mean = 14.3
A24‡
n = 997
mean = 13.7
Count
Frequency (Hz)
C
Right
Anterior
Posterior
Left
Spindle density (min-1)
Monkey MA
MB
MC
Frequency (Hz)
D
Spindle density (min-1)
A46d
A46v
A9
A8a
A8b
A6
SMA
M1
S1
A5
A7
A32
A24
Frequency (Hz)
E
Spindle density (min-1)
r = 0.864
p < 0.0002
Frequency (Hz)

Figure 4

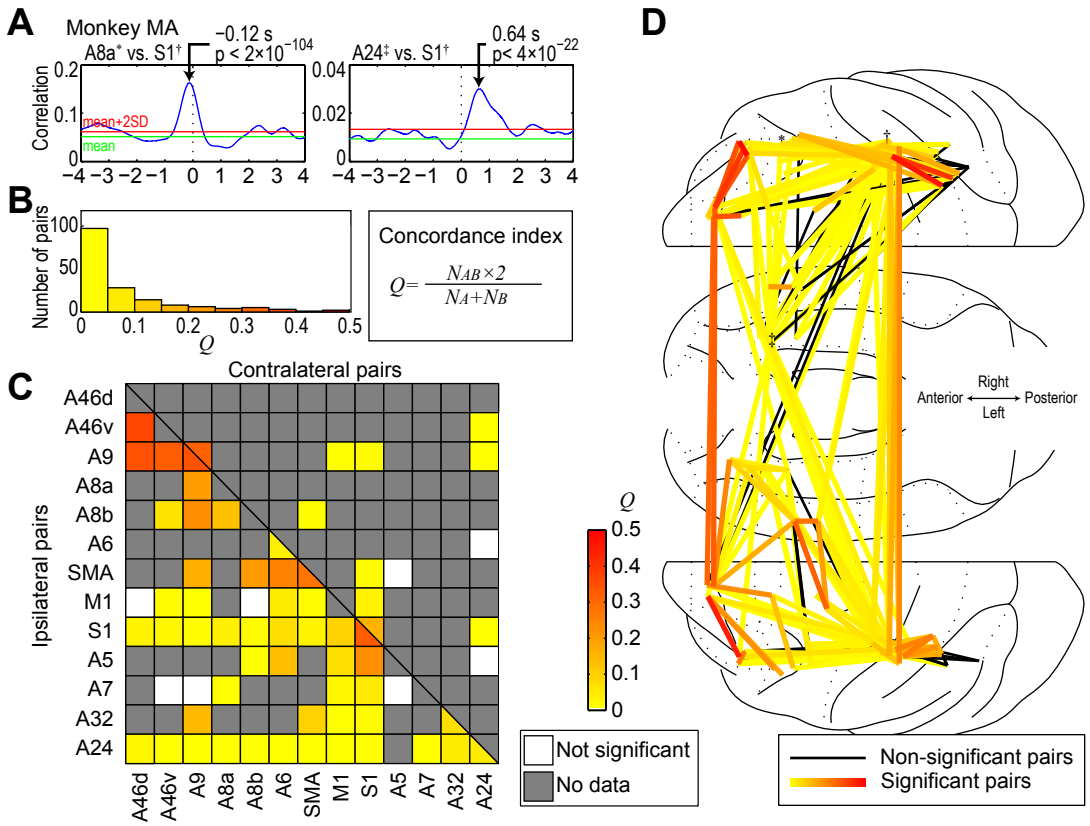
A
Monkey MA
A8a* vs. S1†
−0.12 s
p < 2×10−104
A24‡ vs. S1†
0.64 s
p< 4×10−22
Correlation
mean+2SD
mean
B
Number of pairs
Q
Concordance index
Q= NAB×2 / NA+NB
C
Contralateral pairs
Ipsilateral pairs
A46d
A46v
A9
A8a
A8b
A6
SMA
M1
S1
A5
A7
A32
A24
Q
Not significant
No data
D
Right
Anterior
Posterior
Left
Non-significant pairs
Significant pairs

Figure 5

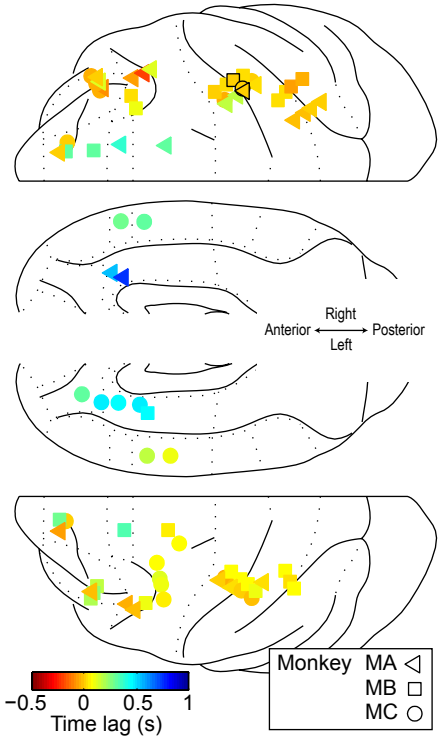
Right
Anterior
Posterior
Left
−0.5
0
0.5
1
Time lag (s)
Monkey
MA
MB
MC

Figure 6

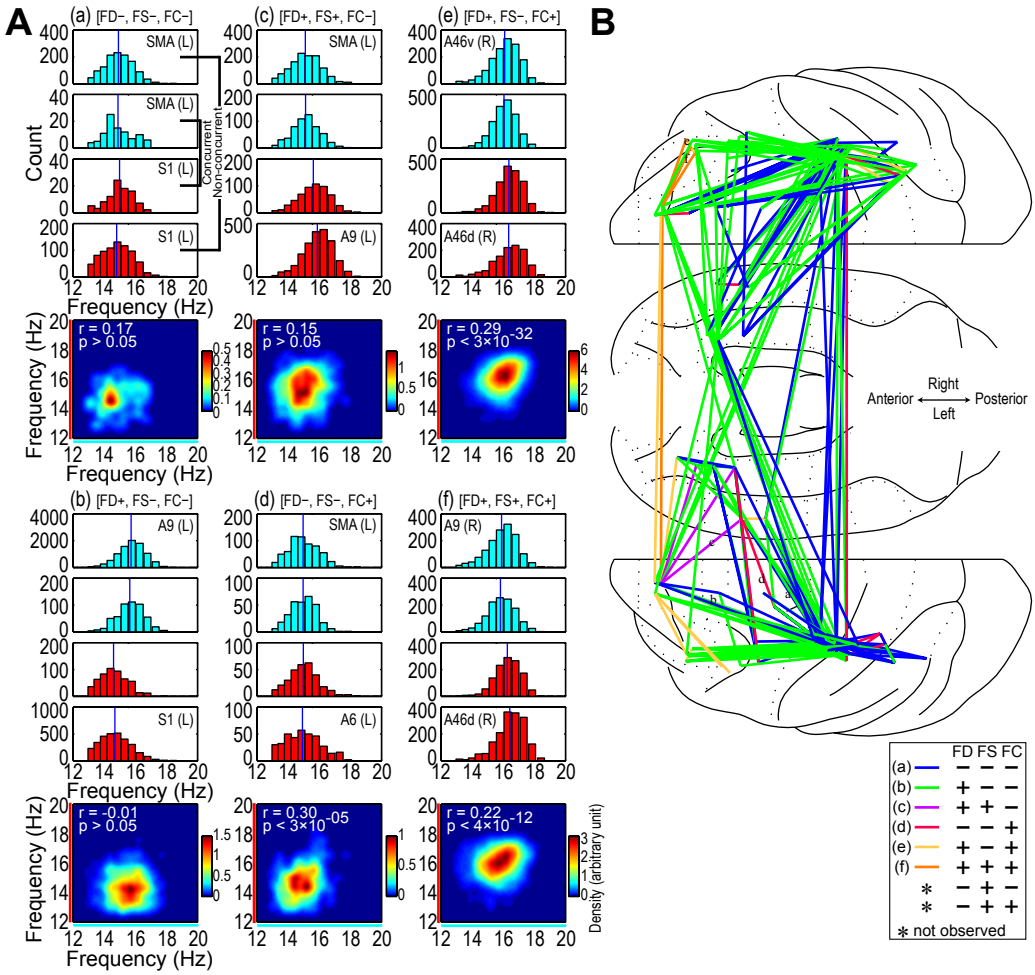
A
B
(a) [FD−, FS−, FC−]
(c) [FD+, FS+, FC−]
(e) [FD+, FS−, FC+]
(b) [FD+, FS−, FC−]
(d) [FD−, FS−, FC+]
(f) [FD+, FS+, FC+]
SMA (L)
S1 (L)
A9 (L)
A46v (R)
A46d (R)
A6 (L)
A9 (R)
Count
Concurrent
Non-concurrent
Frequency (Hz)
r = 0.17
p > 0.05
r = 0.15
p > 0.05
r = 0.29
p < 3×10-32
r = -0.01
p > 0.05
r = 0.30
p < 3×10-05
r = 0.22
p < 4×10-12
Density (arbitrary unit)
Right
Anterior
Posterior
Left
FD FS FC
(a) − − −
(b) + − −
(c) + + −
(d) − − +
(e) + − +
(f) + + +
∗ − + −
∗ − + +
∗ not observed

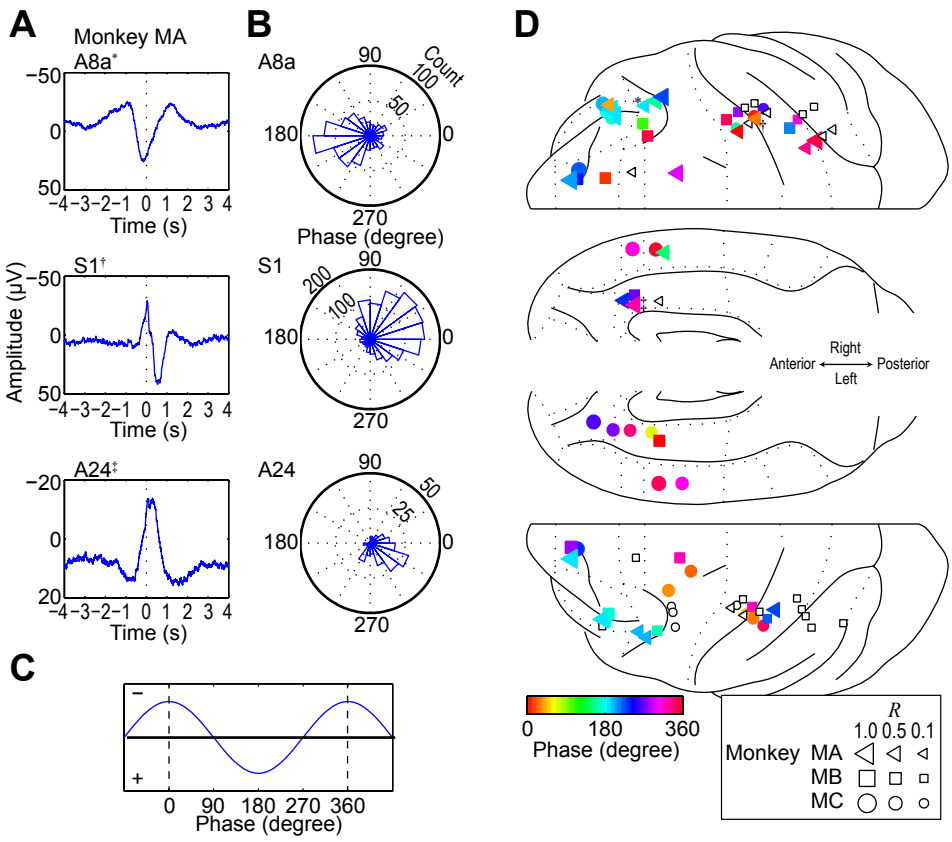
A
Monkey MA
A8a*
S1†
A24‡
Amplitude (μV)
Time (s)
B
A8a
S1
A24
Count
Phase (degree)
C
Phase (degree)
D
Right
Anterior
Posterior
Left
Phase (degree)
Monkey
MA
MB
MC
R
1.0 0.5 0.1

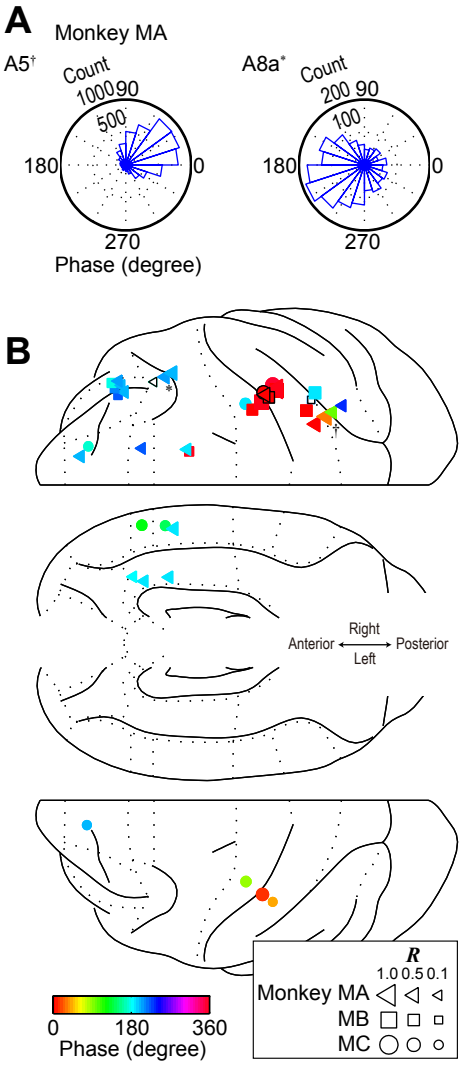
A
Monkey MA
A5†
Count
1000 90
500
180
0
270
Phase (degree)
A8a*
Count
200 90
100
180
0
270
B
Right
Anterior
Posterior
Left
0
180
360
Phase (degree)
R
1.0 0.5 0.1
Monkey MA
MB
MC

Figure 9

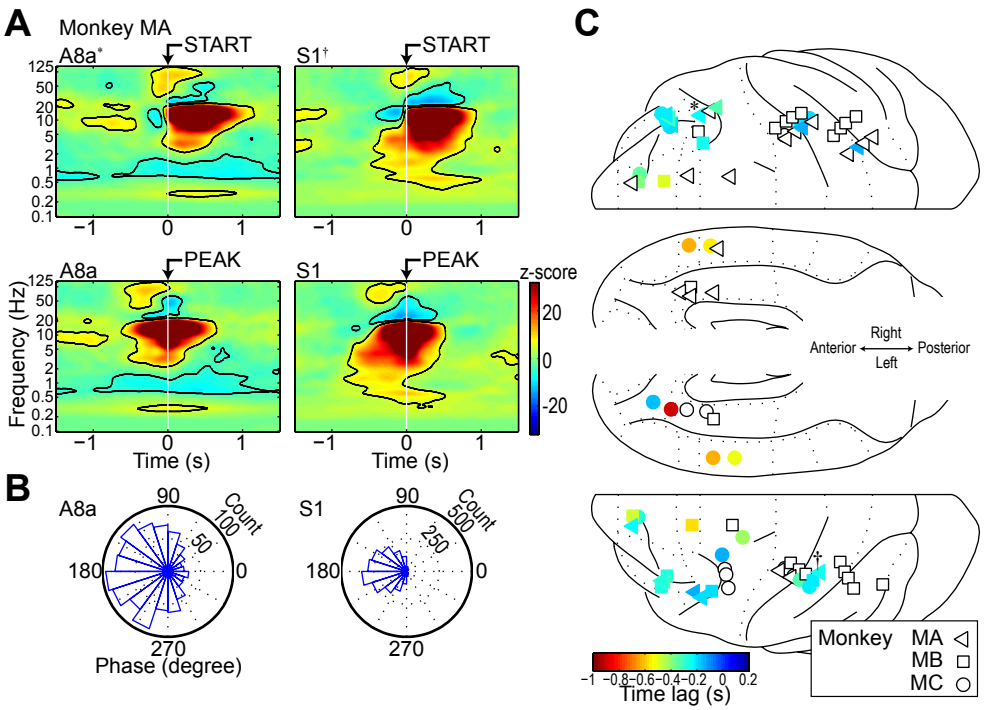
A
Monkey MA
A8a*
START
S1†
START
A8a
PEAK
S1
PEAK
z-score
20
0
-20
Frequency (Hz)
125
50
20
10
5
2
1
0.5
0.2
0.1
−1
0
1
Time (s)
B
A8a
S1
90
180
0
270
Count
100
50
500
250
Phase (degree)
C
Anterior
Posterior
Right
Left
Monkey
MA
MB
MC
−1 −0.8 −0.6 −0.4 −0.2 0 0.2
Time lag (s)